Catalysis Science & Technology

PAPER

View Article Online
View Journal | View Issue

Cite this: *Catal. Sci. Technol.*, 2014, **4**, 3044

Synthesis, acid properties and catalysis by niobium oxide nanostructured materials†

M. Luisa Marin,[ab] Geniece L. Hallett-Tapley,[a] Stefania Impellizzeri,[a] Chiara Fasciani,[a] Sabrina Simoncelli,[ac] José Carlos Netto-Ferreira[ad] and Juan C. Scaiano*[a]

Received 22nd February 2014,
Accepted 8th April 2014

DOI: 10.1039/c4cy00238e

www.rsc.org/catalysis

Several forms of niobium oxide were prepared, including nanostructured mesoporous materials, and their acidity properties were comprehensively investigated and compared with commercially available materials. The composites were characterized by a variety of techniques, including XRD, TEM, N_2 adsorption and Hammett acid indicator studies. The acidity of the niobium oxide derivatives was also investigated by the ability of the materials to successfully promote the halochromic ring-opening of an oxazine-coumarin probe that was specifically designed for use in fluorescence imaging studies. The ring-opening reaction was easily monitored using UV-visible, fluorescence and NMR spectroscopy. Single molecule microscopy was employed to gain a more in-depth understanding of the niobium oxide acid catalysis pathway. Using this technique, the rate of niobium oxide mediated protonation was estimated to be 1.8×10^{-13} mol m^{-2} s^{-1}. Single molecule analysis was also used to obtain a detailed map of Brønsted acid sites on the niobium oxide surface. The active sites, located by multiple blinking events, do not seem to be localized on any area of the material, but rather randomly distributed throughout the solid state surface. As the reaction proceeds, the sites with the highest acidity and accessibility are gradually consumed, making the next tier of acid sites available for reaction. The phenomenon was more closely characterized by using time lapsed reactivity maps.

Introduction

There has been a surge in interest in heterogeneous catalysis over the past decades due to the inherent advantages of using solid catalysts. Such materials can be easily removed from the reaction mixture and also promote the minimization of chemical waste. Hydrated niobium oxide ($Nb_2O_5{\cdot}nH_2O$) is no exception. This amorphous, water tolerant solid acid is comprised of distorted NbO_6 octahedral and NbO_4 tetrahedral geometries,[1,2] with the former responsible for the Brønsted acidity of these materials (equivalent to >70% H_2SO_4) as a result of H_2O coordination to the highly polarized Nb–O (Scheme 1).[1–4]

Due to the remarkable acidity of these materials, many opportunities exist for the use of this solid acid catalyst in a variety of systems where harsher chemicals are typically employed (*e.g.*, concentrated H_2SO_4) and where the removal of excess acid following reaction is desired, but not always feasible. As such, the Brønsted acid character of $Nb_2O_5{\cdot}nH_2O$ has been exploited in the catalysis of many industrially relevant reactions, including esterification,[3] saccharide

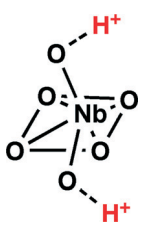

Scheme 1 Distorted octahedral geometry of NbO_6.

[a] *Department of Chemistry and Centre for Catalysis Research and Innovation, University of Ottawa, 10 Marie Curie, Ottawa, K1N 6N5, Canada. E-mail: scaiano@photo.chem.uottawa.ca*
[b] *Instituto Universitario Mixto de Tecnología Química (UPV-CSIC), Universitat Politècnica de València, Avenida de los Naranjos s/n, 46022 Valencia, Spain*
[c] *INQUIMAE and Departamento de Química Inorgánica, Analítica, y Química Física, Facultad de Ciencias Exactas y Naturales, Universidad de Buenos Aires, 1428 Buenos Aires, Argentina*
[d] *Divisão de Metrologia Química, Instituto Nacional de Metrologia, Qualidade e Tecnologia-INMETRO, Duque de Caxias, 25250-020 Rio de Janeiro, Brazil*

† Electronic supplementary information (ESI) available: TEM images of commercial $Nb_2O_5{\cdot}nH_2O$, **T-I**, **T-II**, **T-IIIa**, **T-IIIb** and **T-IV**; XRD spectra of **T-II**, **T-IIIa**, **T-IIIb** and **T-IV**; pore size and surface area data as determined by nitrogen adsorption isotherms; nitrogen adsorption isotherms of commercial $Nb_2O_5{\cdot}nH_2O$, **T-IIIa**, **T-IIIb** and **T-IV**; UV-visible spectra monitoring the Brønsted acid ring opening of **1** to **2** using TFA, **T-II**, **T-IIIb** and **T-IV** as heterogeneous catalysts; fluorescence spectra monitoring the Brønsted acid ring opening of **1** to **2** using TFA, **T-II**, **T-IIIb** and **T-IV** as heterogeneous catalysts; ^{1}H NMR spectra and peak attribution of **1** and **2** in CD_3CN; ^{1}H NMR spectra of **1** in CD_3CN after the addition of **T-IIIa**; diffuse reflectance and solid state fluorescence spectra of product **2** adsorbed onto **T-IIIa**; ^{1}H NMR spectra of **1** in CD_3CN after the addition of **T-I**; experimental set up for single-molecule fluorescence observation under TIRF illumination for the Brønsted acid-catalyzed isomerization of **1** to **2**. See DOI: 10.1039/c4cy00238e

dehydration[3,4] and hydrolysis.[3,5] $Nb_2O_5{\cdot}nH_2O$ holds several advantages over traditional acid catalysts; in addition to ease of removal, the acidity of niobium-based catalysts can be easily tailored using a variety of methodologies. Several studies have examined the effects of temperature on the acidity of $Nb_2O_5{\cdot}nH_2O$, where temperatures lower than 473 K are desired to achieve maximum Brønsted acidity; within conditions above this limit, $Nb_2O_5{\cdot}nH_2O$ Brønsted acidity rapidly decreases due to the increasing crystalline character of the material.[2,6,7] As a result, acid doping of hydrated niobium oxides (*e.g.*; H_3PO_4, HCl, HNO_3)[7,8] has been developed to allow for applications outside of such critical temperature ranges, and has also been exploited as a means of enhancing the acid catalytic capabilities of $Nb_2O_5{\cdot}nH_2O$.

In the current contribution, we explore the properties of a family of five $Nb_2O_5{\cdot}nH_2O$ solids in order to compare the Brønsted acidity of these materials to commercially available alternatives. Initial trials were focused on the characterization of the materials. Later, an emissive halochromic oxazine-coumarin system (**1**) was used to probe the $Nb_2O_5{\cdot}nH_2O$ acidic character with spectroscopic and single molecule microscopy techniques.

Experimental

Materials

Dichloromethane and acetonitrile were purified with a LC Technology Solutions Inc. SPBT-1 Bench-Top Solvent Purification System. Compound **1** was synthesized according to literature procedures.[9] $NbCl_5$ and $Nb(OEt)_5$ used in the preparation of **T-I** and **T-II** were purchased from Sigma-Aldrich and used as received. Commercial Nb_2O_5 (Puratronic®, 99.9985%) was purchased from Alfa Aesar and used as received. Pluronic (P123) and dodecylamine 98% were used as structure-directing agents and were purchased from Sigma-Aldrich. Milli-Q water (resistivity 18.2 MΩ cm^{-1} at 25 °C; 0.22 μm filter) was used in all preparations and reactions requiring aqueous conditions.

Nb_2O_5 modification. Synthesis of the Nb_2O_5 materials discussed within this contribution have been adapted from previously reported procedures. The methods used are briefly described in the following paragraphs:

*$Nb_2O_5{\cdot}nH_2O$ type I (**T-I**).*[10] 5 g of $NbCl_5$ (18.5 mmol) were dissolved in 99% ethanol (10 mL) under constant stirring. To this solution NH_4OH (1 M) was slowly added to the aforementioned solution until a white precipitate was observed. The precipitate was then separated from the solution by centrifugation (3000 rpm), washed four times using Milli-Q water and dried at 120 °C for 24 hours.

*$Nb_2O_5{\cdot}nH_2O$ type II (**T-II**).*[1] 5 g of $NbCl_5$ (18.5 mmol) were dissolved in 200 mL Milli-Q water. Immediately after addition, the yellow powder became white. After stirring for 3 h at room temperature, the white precipitate was centrifuged (3000 rpm) and washed four times with Milli-Q water until the filtrate was at neutral pH. The obtained solid was dried at 120 °C for 24 hours.

*$Nb_2O_5{\cdot}nH_2O$ type III a and b (**T-IIIa and T-IIIb**).*[11] 1.5 g of P-123 were dispersed in 11 mL of Milli-Q water and 45 mL of HCl (2 M) at 40 °C. 5 g of $Nb(OEt)_5$ (15.7 mmol) was added to solution under stirring. The resulting mixture was kept at 40 °C for 24 hours and then precipitated in a Teflon-lined autoclave at 100 °C for 48 hours. The obtained solid was filtered, washed with Milli-Q water and dried in air at room temperature. Excess surfactant was removed by Soxhlet extraction first by washing with 1% HCl in 95% EtOH (300 mL) and then with 95% EtOH only (120 mL). The final, template-free mesoporous $Nb_2O_5{\cdot}nH_2O$ was dried in the oven at 120 °C for 18 hours.

*$Nb_2O_5{\cdot}nH_2O$ type IV (**T-IV**).*[12] A mixture of $Nb(OEt)_5$ (3.25 g, 10.3 mmol) and dodecylamine (0.57 g, 3.1 mmol) was heated until a homogeneous solution was obtained. Subsequent addition of 65.4 mL of Milli-Q water with manual stirring resulted in the formation of a gel-like precipitate. Further addition of 27.6 μL (0.3 mmol) concentrated HCl afforded a white precipitate. The reaction mixture was allowed to stand overnight, sealed and heated at 40 °C for 30 hours, 60–65 °C for 66 hours, 80 °C for 48 hours, and 95–100 °C for 5 days. The solid was then cooled down, collected by filtration and dried at 95–100 °C for 2 hours, 120 °C for 48 hours, and 140 °C for 48 hours. The white solid was then washed four times to remove the presence of excess surfactant. Each washing cycle was conducted for 24 hours under vigorous stirring followed by Büchner filtration. 645 mg (3.4 mmol) of *p*-toluenesulfonic acid in 13 mL of ether were added to 100 mL of MeOH for the first wash. For the second wash, 65 mg (0.3 mmol) of *p*-toluenesulfonic acid in 3 mL of ether were added to 100 mL of MeOH. Third and fourth washings were done using MeOH (100 mL) only. The final, template-free mesoporous $Nb_2O_5{\cdot}nH_2O$ was dried into the oven at 120 °C for 24 hours.

Methods

The synthesis of **1** was monitored by thin-layer chromatography, using aluminum sheets coated with silica (60, F254). NMR spectra were recorded at room temperature with a Bruker Avance 300 instrument. Mass spectral analysis was performed with a 6890N Network GC System equipped with a 5973 Mass Selective Detector from Agilent Technologies. Absorbance spectra were recorded using a Cary 50 UV-visible spectrophotometer. Fluorescence spectra were taken using a Photon Technology International (PTI) spectrofluorimeter using slit widths of 2 nm at the excitation source and 2 nm/5 nm at the detector. Diffuse reflectance spectra were recorded on a Cary 100 UV-visible spectrophotometer fitted with a Labsphere Inc. DRA-30I diffuse reflectance accessory. Nitrogen adsorption/desorption isotherms for the mesoporous Nb oxides were determined from N_2 adsorption at 77 K in an AUTOSORB-6 apparatus. The samples were previously degassed for 4 hours at 523 K and 5×10^{-5} bar. The adsorption branch was used to determine the pore size distribution according to the Barret–Joyner–Helender (BJH) methodology. Mesopore

volume was measured at the plateau of the adsorption branch of the nitrogen isotherm, $P/P_o = 0.8$.[11] Gas adsorption at higher P/P_o is mainly due to interparticle condensation. Small-angle powder X-ray diffraction (XRD) analysis was carried out with a Rigaku Ultima IV diffractometer using a CuKα radiation (k = 1.541836 Å), operating at 40 kV and 30 mA, at a scanning velocity of 0.03° min^{-1} in the $0.7° < 2\theta < 10°$ range. TEM images were acquired using a JEOL JEM-2100F field emission transmission electron microscope equipped with an ultra-high resolution pole piece operating at 200 kV. Thermogravimetric analysis was collected on a TA Instruments Q5000 IR Thermogravimetric Analyzer.

Niobium oxides as Brønsted acid catalysts

Acid strength measurements on the Nb_2O_5 solids discussed in this work were tested using previously published methods.[12,13] In short, 3 drops of a 0.1% solution of each indicator in benzene was added to 100 mg of each material in a clean, dry, 2 mL glass vial. Colour changes were visually observed and recorded as positive (observed indicator colour change) or negative (no observable colour change).

Acid-catalyzed ring-opening of a halochromic oxazine-coumarin probe

Two mg of each Nb_2O_5 solid were placed into a 1 cm × 1 cm quartz cuvette containing 3 mL of a 7.5 μM CH_3CN solution of compound **1**. Each cuvette was sealed to prevent loss of solvent and the absorption and emission spectra were recorded to detect the formation of the ring-opened emissive isomer.

Single-molecule fluorescence microscopy

Imaging fluorescence experiments were performed in a borosilicate reaction chamber with an area of 4.2 cm^2 per well (Thermo Scientific). Coverslips (18 mm × 18 mm; Fisher Scientific) were cleaned in piranha solution (1 : 3 H_2O_2 : H_2SO_4) for 1 hour and then rinsed thoroughly with water. The slides were dried with N_2 prior to functionalization. The surface was functionalized by spin coating a dispersion of **T-I** in methanol (2 mg in 2 mL) at 1000 rpm for 40 s. The cover slides were then placed in the chamber and submerged in 1 mL of Milli-Q water, to which 2 μL of a 10 nM solution of compound **1** in CH_3CN were added. TIRF images were acquired on an Olympus FV1000 TIRF microscope (Olympus; Japan) using an oil immersion Plan Apo objective 100× NA1.45 (Olympus; Japan) and a highly sensitive Rolera EM-C^2 camera (Q-Imaging, Surrey, Canada). TIR illumination was achieved by focusing a 633 nm He–Ne, CW laser onto the back focal plane of the objective. The power density of the excitation laser at the sample was estimated to be 40 W cm^{-2}. A Chroma ET600 excitation filter was used (Chroma Technology Corporation, Bellows Falls, USA). The emission was collected by a camera after direction through a dichroic mirror (Chroma ZT640) and an emission filter (Chroma ET655) to remove light from the excitation source. The pixel size of the image corresponds to 156 nm. Fluorescence spectra were recorded with a Fluorescent Lifetime Imaging System (PicoQuant, Berlin, Germany). The instrument is equipped with a frequency doubled, picosecond pulse diode laser (637 nm, 93 ps, 40 MHz, LDH-P-FA-640L; PicoQuant). The laser beam was collimated and focused through a fiber-coupling unit. A beam splitter (Z638rdc, Chroma) was used to separate excitation and emission light. The emission signal was collected by a Shemrock SR-163 spectrograph (Andor Technology, South Windsor, USA).

Results and discussion

$Nb_2O_5{\cdot}nH_2O$ characterization; TEM, XRD and nitrogen adsorption isotherms

Synthetic $Nb_2O_5{\cdot}nH_2O$ T(I-IV), as well as the commercially available $Nb_2O_5{\cdot}nH_2O$ were characterized to gain a thorough understanding of the acidic characteristics of these materials. The crystalline state of $Nb_2O_5{\cdot}nH_2O$ is well known to directly influence the Brønsted acidity of these materials,[2,6,7] therefore TEM images were obtained of all six samples (Fig. S1, ESI†). Analysis of the TEM images appears to illustrate an amorphous solid in all cases, typical of hydrated niobium oxides and necessary for achieving optimal Brønsted acidity. The amorphous nature of the $Nb_2O_5{\cdot}nH_2O$ was more closely examined using XRD spectroscopy. As can be observed in Fig. 1, the XRD patterns obtained following analysis of the commercial $Nb_2O_5{\cdot}nH_2O$ sample and **T-I** are considerably different. Specifically, the XRD spectrum of the commercial solid presents sharp defined diffraction peaks, while that of the synthesized derivative presents two broad diffraction peaks at approximately 25° and 53°. Likewise, XRD spectra obtained for **T-II** to **T-IV** (Fig. S2, ESI†) also present broadened diffraction patterns, with the mesoporous materials showing one diffraction at approximately 2.5°. Such broadening of the XRD diffraction patterns is characteristic of amorphous solids supporting the conclusions drawn from TEM imaging, and suggesting that the five synthetically prepared niobium oxides may be useful as Brønsted acid catalysts. Conversely, XRD spectroscopy indicates that the commercial $Nb_2O_5{\cdot}nH_2O$ is more crystalline in nature, illustrated by the well-defined diffraction pattern. Such attributes suggest that this material may be considerably less acidic than the synthesized derivatives.

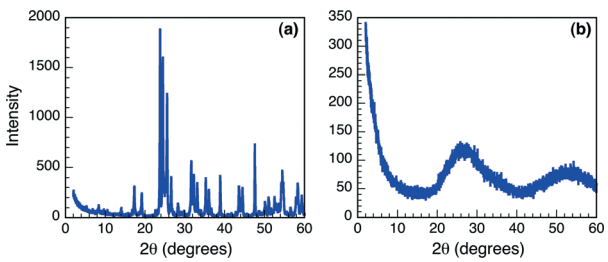

Fig. 1 XRD spectra of (a) commercial $Nb_2O_5{\cdot}nH_2O$ and (b) **T-I**.

The pore size of the mesoporous materials (**T-III** and **T-IV**) was assessed using nitrogen adsorption isotherms due to the distinctive nitrogen uptake as a result of the capillary condensation of nitrogen inside of the mesopores. Table S1 (ESI†) presents the average surface area and pore size as calculated from the isotherm data for the three niobium oxide materials with mesoporous structure and demonstrates the porosity of the solids. Importantly, the overall surface area and pore size variations are not only dependent on the method of preparation, but also tend to vary from batch to batch within the same synthetic methodology, as shown for **T-IIIa** and **T-IIIb**. Both of these mesoporous niobium oxides were prepared using P-123 as a templating agent; nonetheless, the surface area (528 $m^2\ g^{-1}$ and 295 $m^2\ g^{-1}$, respectively) and pore size (24.4 Å and 9.57 Å) are significantly different, trends that are not uncommon in mesopore synthesis.[14] As such, both solids were employed for further testing as Brønsted acid catalysts.

Assessment of niobium oxide acidity

In order to assess and quantify the overall acidity of both the commercial and synthesized niobium oxides, both acid indicator studies and thermogravimetric analysis (TGA) of the samples were undertaken. The acidity of solid samples is commonly reported as a function of Hammett acidity (H_0).[15] Using this method, the solid samples are placed in the presence of indicator dyes with known pK_a values, allowing for one to establish a defined pK_a range for the sample of interest. Preliminary assessments of the acidity of the niobium oxide materials were carried out using six indicators. The indicators and respective results obtained by this method of qualitative testing are reported in Table 1, which shows that the pK_a range of the $Nb_2O_5{\cdot}nH_2O$ are largely variable, with the commercial Nb_2O_5 being the least acid with $H_0 > +5.0$. The tabulated Hammett acidity values clearly illustrate that all of the synthesized $Nb_2O_5{\cdot}nH_2O$ are acidic in nature.

Assessment of niobium oxide thermal stability

Knowing that increasing temperatures greatly affects the crystallinity, and, thus, Brønsted acidity of the $Nb_2O_5{\cdot}nH_2O$ matrix, thermogravimetric analysis was carried out to examine the influence of increasing temperature on the aforementioned solid samples. The TGA traces obtained over a 500 °C temperature range are reported in Fig. 2. The traces illustrate that **T-I** undergoes the largest thermal degradation, as is represented by the largest loss of sample mass (% weight), followed by **T-IIIa** and there is no weight loss from the commercial sample. These results seem to suggest that the commercial Nb_2O_5 is the most robust material to be examined in this study and the least affected by temperature. Moreover, the TGA results suggest that the commercial sample is considerably crystalline in nature and, as such, void of any Brønsted acid characteristics, as corroborated by the indicator studies. All other $Nb_2O_5{\cdot}nH_2O$ samples showed some thermal degradation upon exposure to extreme temperature conditions, which may be due in part to changes in the physical properties of the solid state matrix (*i.e.* amorphous to crystalline), loss of mesoporous structure and also partially due to loss of H_2O, as H_2O coordination is critical in Brønsted acidity activation in Nb_2O_5.[2,7]

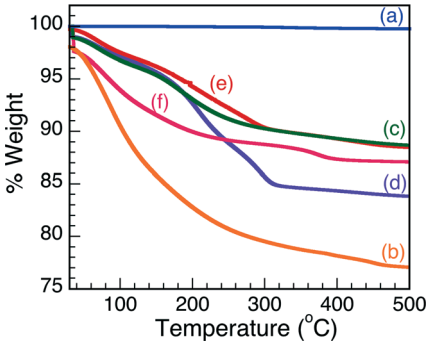

Fig. 2 Thermogravimetric analysis of (a) comm. $Nb_2O_5{\cdot}nH_2O$, (b) **T-I**, (c) **T-II**, (d) **T-IIIa**, (e) **T-IIIb** and (f) **T-IV**.

Catalytic $Nb_2O_5{\cdot}nH_2O$ fluorescence activation

The design of the halochromic compound **1** is based on the established properties of switchable oxazines. These compounds are known to switch reversibly between isomeric states with distinctive structural properties and spectroscopic signature upon light or chemical stimulation.[16] Covalent conjugation of the oxazine moiety with a coumarin fluorophore generates an emissive switchable bimolecular system, in which the fluorescence of the latter can be modulated in response to the pronounced structural and electronic modifications associated

Table 1 Hammett acidity (H_0) for $Nb_2O_5{\cdot}nH_2O$[a]

Indicator	Max. pK_a	Comm. Nb_2O_5	T-I	T-II	T-IIIa	T-IIIb	T-IV
Methyl red	+5.0	−	+	+	+	+	+
Methyl yellow	+3.3	−	+	+	+	+	+
Crystal violet	+0.8	−	+	+	+	+	+
Dicinnamal-acetone	−3.0	−	−	+	+	+	+
Chalcone	−5.6	−	−	+	+	+	−
Anthraquinone	−8.6	−	−	−	−	−	−
H_0		> +5.0	−3.0 to +0.8	−8.6 to −5.6	−8.6 to −5.6	−8.6 to −5.6	−5.6 to −3.0

[a] (+) = observable colour change; (−) = no observable colour change.

with either the photo- or chemically induced transformation of the former.[9,17]

The absorption spectrum of **1** in CH_3CN shows a band centered at 410 nm. The addition of acid, such as trifluoroacetic acid (TFA), opens the oxazine ring and permanently generates compound **2** (Fig. 3). Within this transformation, the coumarin functionality is brought in conjugation with the cationic fragment of the generated isomer, shifting its absorption band bathochromically by *ca.* 180 nm. A fluorescence band centered at 645 nm can then be observed by selectively exciting **2** at λ_{ex} of 530 nm. Therefore, the transformation of **1** into **2**, encouraged by the addition of acid, can be exploited to activate fluorescence and allows the investigation of materials with distinctive acidic properties with relatively simple experimental setups.

The use of an emissive probe with switchable character offers several advantages with respect to other pH-sensitive fluorophores (*e.g.* coumarin-6) which are strongly emissive either before or after the addition of acid and show only a discrete shift of the emission wavelength in response to protonation.[18] The observation of stimuli-generated fluorescence in a dark background (such is observed for **1**), rather than the shifting of the emission of a fluorescent substrate (coumarin-6), offers the opportunity to image fluorescent elements with improved signal to noise ratio, allowing the detection and identification of structural features with higher precision and the investigation of $Nb_2O_5{\cdot}nH_2O$-mediated acid catalysis at the molecular level.

To further investigate the niobium oxides discussed herein as Brønsted acid catalysts, 2 mg of each solid were placed in 3 mL of a 7.5 μM CH_3CN solution of compound **1**. In all cases, the reaction mixture rapidly changed colour

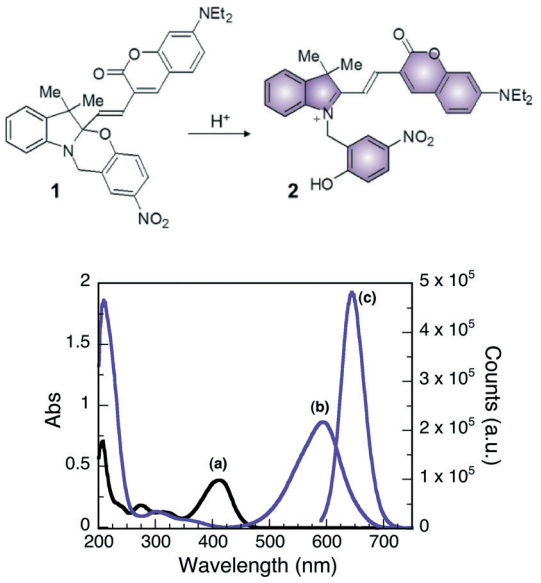

Fig. 3 (Top) Structures of **1** and **2**. (bottom) Absorption spectra of **1** (10 μM, CH_3CN, 25 °C) before (a) and after (b) the addition of 10 equivalents of TFA. Emission spectrum (c, λ_{ex} = 570 nm, CH_3CN, 25 °C, right scale) of **1** after the addition of 10 equivalents of TFA.

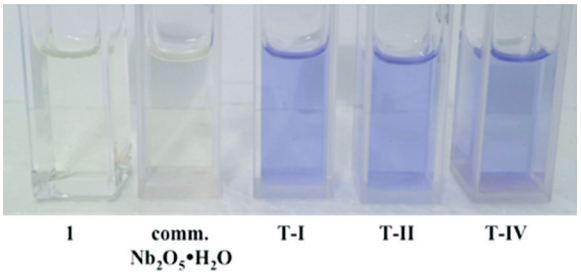

Fig. 4 Photographs illustrating the colour change observed upon ring opening of **1** in the presence of Brønsted acidic $Nb_2O_5{\cdot}nH_2O$.

(from pale yellow to blue/purple) upon the addition of the five synthesized $Nb_2O_5{\cdot}nH_2O$ materials (Fig. 4), indicating the formation of **2** upon ring-opening reaction, while the addition of commercial Nb_2O_5 resulted in no observable colour change. These results support the absence of Brønsted acidity in the commercial niobium sample. Trifluoroacetic acid was also used as a control and yielded positive results.

The halochromic opening of **1** was monitored using both absorption and fluorescence spectroscopy. Fig. 5 and S4 (ESI†) present the UV-visible spectra obtained upon addition of TFA or the $Nb_2O_5{\cdot}nH_2O$ catalysts discussed in Table 1. TFA was first added to a CH_3CN solution of oxazine-coumarin **1** as a control experiment. The reaction immediately turned deep blue in colour and was left to equilibrate for 1 h. Subsequent spectroscopic measurements revealed a shift in the absorption spectrum from 410 nm to 595 nm (Fig. S4A†), due to the formation of **2**, which slowly continued over the monitoring period of 5 days. Similarly, the niobium oxide catalysts presented in Table 1 were added to a fresh solution of **1**. Implementing commercial Nb_2O_5 as a heterogeneous Brønsted acid catalyst afforded no appreciable change in the absorption maximum (Fig. 5A), indicating no conversion to

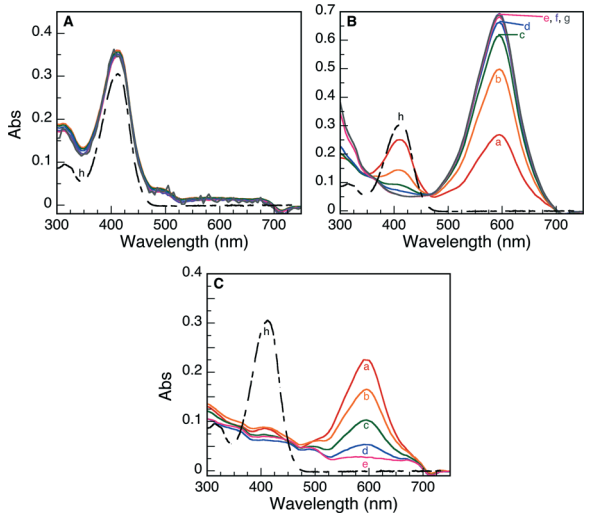

Fig. 5 UV-visible spectra monitoring the Brønsted acid-induced ring opening of **1** to **2** using (A) commercial $Nb_2O_5{\cdot}nH_2O$, (B) **T-I** and (C) **T-IIIa** as heterogeneous catalysts. The reactions were monitored as a function of time: (a) 0 h, (b) 1 h, (c) 3 h, (d) 5 h, (e) 24 h, (f) 3 d, (g) 5 d and (h) initial absorption of **1**.

the ring-opened isomer **2**. The results obtained using the commercial sample further suggest that this $Nb_2O_5{\cdot}nH_2O$ is void of any Brønsted acid properties.

In the case of the five synthetically prepared $Nb_2O_5{\cdot}nH_2O$ catalysts, a distinct variation in the UV-visible spectrum was detected upon addition of each heterogeneous material to a solution of the oxazine-coumarin probe **1**. Following addition of **T-I** and **T-IIIa** as Brønsted catalysts (Fig. 5B and C), a subsequent shift in the absorption spectrum was observed, similar to that seen in TFA control studies, indicative of oxazine ring-opening to form compound **2**. In the case of catalyst **T-I**, the formation of **2** slowly progresses over 5 days, whereas when catalyst **T-IIIa** was employed, rapid formation of **2** was preceded by a gradual decrease of the absorption band ascribed to ring-opened isomer **2** (the decrease in the observed absorbance is only attributed to adsorption on the catalyst surface rather than hydrolysis of **2** as is illustrated by the control experiments presented in Fig. S5†).

Moreover, after 5 days, both catalysts appeared blue in colour, implying that adsorption of the probe molecule onto the acidic sites of the $Nb_2O_5{\cdot}nH_2O$ catalysts is integral in the catalytic ring-opening process. The more rapid decline in the absorption of **2** in the presence of **T-IIIa** may be simply due to the mesoporous nature of this material and the more rapid and favourable adsorption of the probe molecule into the support matrix.

Results similar to **T-IIIa** were obtained for the remaining three $Nb_2O_5{\cdot}nH_2O$ solids (**T-II**, **T-IIIb** and **T-IV**) and are presented in Fig. S4.† In all cases, the solid catalyst turned blue after 5 days of reaction and the absorption spectra attributed to ring-opened oxazine **2** decreased as a function of monitoring time, again suggesting that adsorption of the probe onto the catalyst surface may constitute a fundamental step in the catalysis pathway.

The formation of the emissive isomer **2** was also monitored *via* fluorescence spectroscopy. An appearance of fluorescence at 645 nm following the addition of TFA (Fig. S6A†) resulted from protonation of compound **1** to generate **2**, which continued to form over the timescale of the experiment (4 days). Fig. 6 presents the emission spectra obtained when commercial $Nb_2O_5{\cdot}nH_2O$, **T-I** and **T-IIIa** were added as heterogeneous Brønsted acid catalysts. These trends closely mimic those observed for UV-visible spectroscopy, where no changes in the fluorescence spectra were observed when the commercial material was used (over a monitoring period of 4 days). On the other hand, an emission band at 645 nm was detected after 1.5 h following addition of both **T-I** and **T-IIIa**. The emission at 645 nm slowly increased as a function of time in the presence of **T-I**. On the contrary, rapid protonation of **1**, followed by an ensuing decrease in intensity of the 645 nm emission over 4 days, was observed for catalyst **T-IIIa**.

Fig. S6† presents the remaining fluorescence spectra for $Nb_2O_5{\cdot}nH_2O$ **T-II**, **T-IIIb** and **T-IV**. In all cases, protonation of **1** manifests as the growth of a fluorescence band at 645 nm due to formation of compound **2**; however, the emission

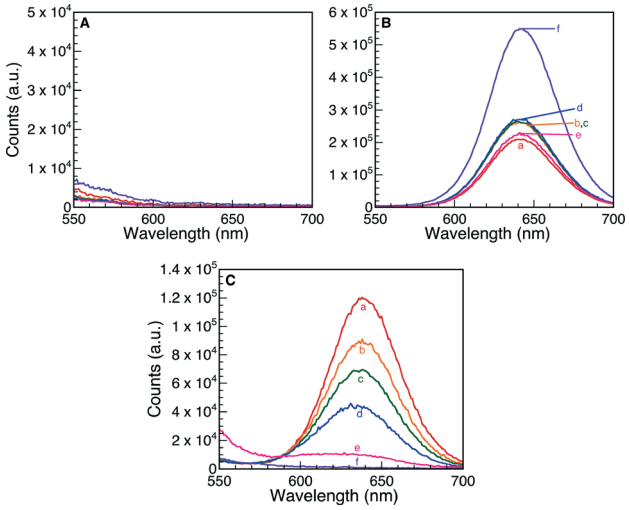

Fig. 6 Fluorescence spectra monitoring the Brønsted acid ring opening of **1** to **2** using (A) commercial $Nb_2O_5{\cdot}nH_2O$, (B) **T-I** and (C) **T-IIIa** as heterogeneous catalysts. The reactions were monitored as a function of time: (a) 1 h, (b) 3 h, (c) 4 h, (d) 6 h, (e) 30 h and (f) 4 d. Note changes in vertical scale in the various panels.

progressively decreases over 4 days, likely due to adsorption of ring-opened oxazine **2** onto or into the support matrix.

As previously discussed, the change in colour of the synthetically-prepared $Nb_2O_5{\cdot}nH_2O$ catalysts, in conjunction with the observed variations in both the UV-visible and fluorescence spectra over time, seems to indicate a permanent adsorption of the probe onto the support surface. The rate at which this process occurs was found to be dependent upon the catalyst used, where the mesoporous $Nb_2O_5{\cdot}nH_2O$ (**T-IIIa**, **T-IIIb** and **T-IV**) demonstrated more rapid adsorption, likely due to incorporation of the molecule into the porous structure. In order to further investigate this process, time-lapsed ^{1}H NMR was performed on a solution of **1** following the addition of **T-IIIa** in CD_3CN. Although the solution coloured instantaneously, the ^{1}H NMR spectrum (Fig. S8a, ESI†) shows broadened peaks that can be only attributed to the starting material **1** (Fig. S7†), and not to its protonated form **2** (chemical shifts from **2** can be observed by adding 10 equivalents of TFA to a solution of **1** in CD_3CN, Fig. S7†). The spectra in Fig. S8† represent only the 8.5 to 4 ppm region of the NMR to allow for a more specific comparison of the peaks that are relevant to this discussion. Further confirmation of the exclusive presence of **1** is provided by the analysis of the diastereotopic protons H_y and H_z, which are known to shift from 4.7 ppm in **1** to 5.8 ppm in **2** (Fig. S7 and S8†). In addition, the signals decrease in intensity and lose definition over time (Fig. S8b–d), in agreement with the previous observation of increasing colouration of the solid material. The solid catalyst was separated by centrifugation and analyzed by diffuse reflectance and fluorescence spectroscopy; the corresponding spectra (Fig. S9†) illustrate the presence of a broad band centered at ~630 nm and a broad emission centered at 720 nm, respectively, further confirming the adsorption of compound **2** onto the support surface. Broadening of absorption and

emission curves when measured in the solid state is commonly observed due to differing dielectric constants of the solvent and solid state media.[19]

In order to test the proposal that the halochromic probe was, in part, incorporated into the mesopores of **T-IIIa** (as suggested by absorption and emission spectroscopy), time-controlled ^{1}H NMR analysis of a mixture of **1** and the non-mesoporous **T-I** was also carried out for comparison. In the case of **T-I**, broad signals were also detected that can be attributed to **1**, together with the progressive diminution of their intensity (Fig. S10†) and the contemporaneous colouration of the solid catalyst. However, no noteworthy variations in the NMR spectrum could be observed 2 h after catalyst addition (Fig. S10b†), while ^{1}H signals are already significantly different from the initial recordings (Fig. S8b†) 2 h after the addition of **T-IIIa**. These results confirm that compound **1** adsorbs differently on the catalyst surface depending on the type of $Nb_2O_5{\cdot}nH_2O$ used, as was also observed during spectroscopy measurements (Fig. 5, 6, S4 and S6†). Furthermore, measurements performed using **T-IIIa** show that the chemical shifts remained constant for the duration of the experiment (up to 96 hours, with signals that are barely visible), whereas after 4 days from the initial addition of **T-I** to **1**, the ^{1}H NMR peaks shift to resemble those of **2** (Fig. S10c;† as compared with the TFA control). This comparative study suggests that in the case of **T-IIIa**, product **2** has likely been incorporated into the pores of the material.

Based on these observations, compound **1** is believed to be initially adsorbed onto the surface of the catalyst (due to the total absence of ^{1}H NMR signals from **2**) and, once adsorbed, to undergo the proposed Brønsted acid catalyzed ring-opening reaction directly on the surface to generate **2**. The instantaneous purple/blue colouration of the solution when the niobic acid catalysts are added to **1** is attributed to an initial stage of the reaction, where the blue colouration is likely the result of a combined effect that includes the reaction of molecules in close proximity to the most exposed acidic sites on the catalyst surface, and the large absorption extinction coefficient of product **2**.[9]

Recyclablity of the $Nb_2O_5{\cdot}nH_2O$ catalysts was also briefly examined using catalyst **T-I** as the probe. This particular composite was chosen due to its lack of mesoporosity, thus eliminating consideration of substrate adsorption into the pores of the material. As is shown in Fig. S11,† the amount of ring-opened product **2** obtained following one reuse of the material suggests good catalyst reusability and minimal loss of the $Nb_2O_5{\cdot}nH_2O$ acidic properties.

Catalysis at the single molecule level

The catalytic protonation of compound **1** (and ring opening) over **T-I** was investigated by allowing the exposure of the particles to the reagent solution while monitoring the fluorescence signal of the product in a TIRF microscope (Fig. S12†). **T-I** dispersed in methanol was deposited on a cleaned cover glass by spin coating and then mounted at the bottom of a 1.25 mL reaction chamber. The particles were immersed in 1 mL of Milli-Q water. Upon addition of 2 μL of a 100 nM CH_3CN solution of compound **1**, bright fluorescent spots appeared over the particles (Fig. 7). Catalytic sites over the particles were reconstructed by accumulating the spot intensity of a movie of 500 frames in length (frame time = 100 ms). The 3D representation of the active sites (Fig. 7, right) shows that events are detected all over the particle without having a preferred position. A fraction of the sites on the catalyst surface seems to be responsible for the activity.

Typical trajectories at selected bright spots are shown in Fig. 8A. Characterization of bright spots was performed by measuring the emission spectra *in situ* (Fig. 8C), ascribed to product **2**. No fluorescent events were observed in control experiments performed without catalyst or without reagent or in the surrounding solution when compound **1** was added, indicating that the formation of the fluorescent product **2**

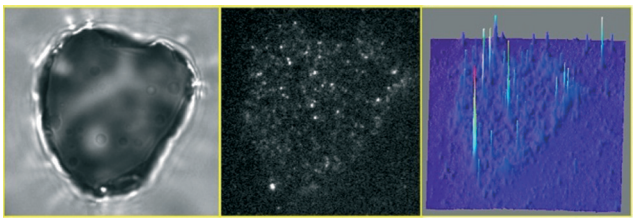

Fig. 7 Transmission (left) and TIRF (center) images of the same **T-I** particle immobilized on a cover glass and immersed in a 0.2 nM solution of compound **1** with 633 nm laser excitation (see ESI† Video S1). (Right) 3D representation of the accumulated spot intensity over the same particle reconstructed from a movie of 500 frames in length (frame time = 100 ms).

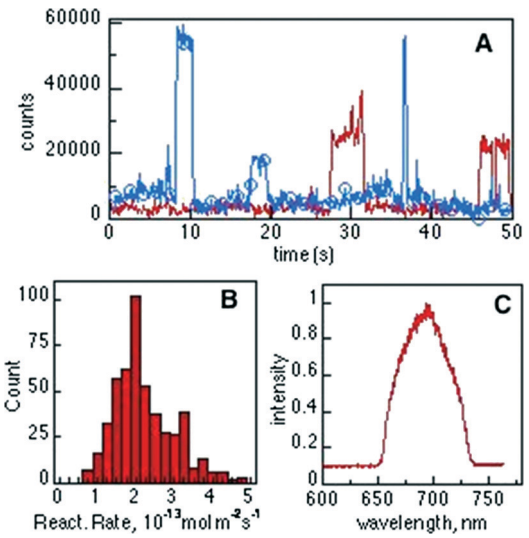

Fig. 8 (A) Typical fluorescence intensity trajectories observed for the "turn ON" of molecules of product **2** over a single **T-I** particle. (B) Distribution of initial reaction rates for the Brønsted acid-catalyzed transformation of compound **1** into **2** (n = 500) and (C) spectral information of the detected bright spots during "turn ON" events measured by passing the epi fluorescent signal through a spectrograph.

can only be attributed to the Brønsted acidity of the **T-I** catalyst. Counting the single "turn ON" events of fluorescent molecules over the catalyst allows for an estimation of the reaction rate constant for the Brønsted acid-catalyzed ring opening of compound **1** and was found to be ~1.8×10^{-13} mol m^{-2} s^{-1}, as illustrated in Fig. 8B.

The diffusion coefficient of a small molecule in water, for example of fluorescein, is in the order of 5×10^{-6} cm^2 s^{-1},[20] thus, within the TIRF excitation region (~200 nm) the diffusion time is on the μs timescale, being much shorter than the 100 ms imaging frame of our experiments. However, the ON time distribution histogram (not shown) shows an average ON time of around 2.5 s. This observation leads to the assumption that molecules of product **2** reside over the Nb_2O_5 catalyst sites and are observable before photobleaching occurs.

Deactivation of catalyst activity is an important concern for industry applications of any type of catalytic reaction and therefore using microscopic techniques for analyzing adsorption of the product is of wide importance.

In order to establish how robust the catalytic sites are, we carried out a study in which a sequence of 500 images was treated as in Fig. 7 (right), but accumulating separately the first 250 images from the subsequent set of 250 images. This corresponds to two sets of 25 seconds each as shown in Fig. 9, for a data set different from that in Fig. 7 (maps for the spot in Fig. 7 are available in Fig. S13†). Subtraction of the two sets gives the image shown in Fig. 9C and from a side-view in Fig. 9D, where positive signals represent loss of activity and negative signals activity gained. We were initially puzzled by the latter observation, as we did not expect additional acid sites to appear or be released with time.

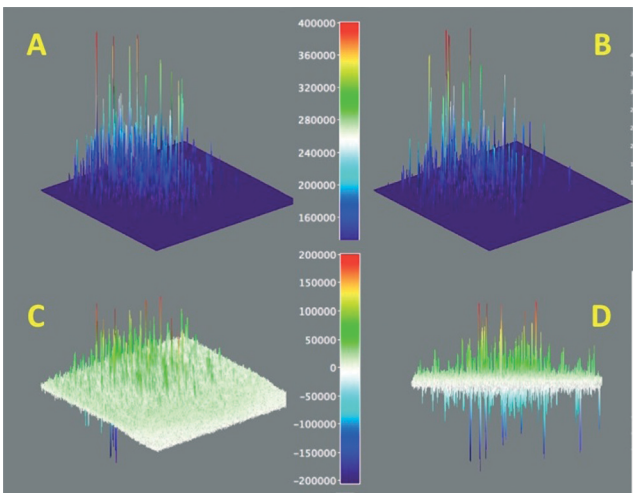

Fig. 9 Protonation activity as shown by the conversion of **1** → **2** and detection of the fluorescence from **2**. Surface maps A and B show the accumulated signals for 25 seconds and the subsequent 25 seconds, while map C shows the difference of A minus B expanded approximately ×2 (see colour coded scale). Panel D shows a different view of panel C, showing positive and negative peaks. Note that this figure is for a different spot than that in Fig. 7.

Interestingly, statistics calculated from Fig. 9D show that the average of all peaks is approximately zero within experimental error; this means that active sites that become inactive are replaced by new sites nearby. As we are using diffraction-limited optical methods, this effectively means new sites are ~300 nm or more from sites losing activity. Sites that appear at the same location will not be counted in this method as their bright blinks simply replace the previous ones. Visual analysis of enlarged images suggest that new sites are not very far from old ones. The simplest interpretation is that early acidity maps reveal hot spots on the catalyst, where 'hot spots' are characterized by their high acidity and easy accessibility; as these are used up by the chemistry of Fig. 3, the next tier of sites becomes active, effectively appearing in these maps as if acid sites had been created, when in fact they were available all along, they simply become active as their better competitors are used. We find that the time-lapse maps of Fig. 9 are a convenient representation of what otherwise can only be examined from TIRF videos.

Conclusions

Five $Nb_2O_5 \cdot nH_2O$ materials have been synthesized using a combination of both literature and newly developed synthetic procedures. These materials were determined to be amorphous in nature by way of XRD and TEM imaging, while N_2 adsorption studies confirmed the mesoporous characteristics of samples **T-III** and **T-IV**. Acid indicator studies employing the Hammett acidity function of all the samples discussed within this contribution confirmed the acidic nature of the five synthesized $Nb_2O_5 \cdot nH_2O$ materials. Surprisingly, the commercial Nb_2O_5 was found to be void of any acidic characteristics. Commercial Nb_2O_5 and $Nb_2O_5 \cdot nH_2O$ **T-I–T-IV** were tested in the halochromic ring opening of oxazine-coumarin **1**. The prepared $Nb_2O_5 \cdot nH_2O$ derivatives rapidly converted oxazine-coumarin **1** to the open-form **2**, as was observed in both UV-visible and fluorescence spectroscopy, while commercial Nb_2O_5 was found to be inactive in this reaction, likely due to its lack of acidic properties. Through NMR spectroscopy, the ring-opening of **1** was suggested to require adsorption of the closed form **1** onto the material surface to facilitate effective substrate protonation and form the Brønsted acid catalyzed ring opened product **2**. Total internal reflectance microscopy was used to monitor the acid induced ring opening of **1** with single molecule resolution. The rate constant for the Brønsted acid catalyzed coumarin-spyrooxazine ring opening was estimated to be 1.8×10^{-13} mol m^{-2} s^{-1}. Moreover, using single molecule techniques, it was determined that the adsorption of substrate **1** and subsequent ring opening is distributed over the $Nb_2O_5 \cdot nH_2O$ surface, with the emissive open form **2** exhibiting an average ON time of 2.5 s. The reaction is suggested to proceed with a gradual exchange of the initial 'hot spots', characterized by high acidity and easy accessibility, for the next tier of acid sites as the most reactive locations are depleted.

Acknowledgements

The authors wish to thank the Natural Sciences and Engineering Research Council (NSERC) and the Canada Research Chairs program. The University of Ottawa International Office provided grants to study niobium. M. L. Marin thanks the financial support of the Generalitat Valenciana (BEST/2012/233). Thanks are due to the Government of Canada and NSERC for a Banting Postdoctoral Fellowship to S. Impellizzeri and a Vanier Sholarship to C. Fasciani. S. Simoncelli acknowledges a DFAIT fellowship from ELAP (Emerging Leaders in the Americas Program) to support her visit to Canada.

Notes and references

1 K. Nakajima, Y. Baba, R. Noma, M. Kitano, J. N. Kondo, S. Hayashi and M. Hara, *J. Am. Chem. Soc.*, 2011, **133**, 4224–4227.
2 I. Nowak and M. Ziolek, *Chem. Rev.*, 1999, **99**, 3603–3624.
3 K. Tanabe and S. Okazaki, *Appl. Catal., A*, 1995, **133**, 191–218.
4 T. Armaroli, G. Busca, C. Carlini, M. Giuttari, A. M. R. Galletti and G. Sbrana, *J. Mol. Catal. A: Chem.*, 2000, **151**, 233–243; C. Carlini, M. Giuttari, A. M. R. Galletti, G. Sbrana, T. Armaroli and G. Busca, *Appl. Catal., A*, 1999, **183**, 295–302.
5 G. S. Nair, E. Adrijanto, A. Alsalme, I. V. Kozhevnikov, D. J. Cooke, D. R. Brown and N. R. Shiju, *Catal. Sci. Technol.*, 2012, **2**, 1173–1179; M. Marzo, A. Gervasini and P. Carniti, *Carbohydr. Res.*, 2012, **347**, 23–31.
6 E. I. Ko and J. G. Weissman, *Catal. Today*, 1990, **8**, 27–36.
7 S. Okazaki and A. Kurosaki, *Catal. Today*, 1990, **8**, 113–122; S. Okazaki and N. Wada, *Catal. Today*, 1993, **16**, 349–359.
8 T. Ushikubo, I. Iizuka, H. Hattori and K. Tanabe, *Catal. Today*, 1993, **16**, 291–295.
9 E. Deniz, S. Sortino and F. M. Raymo, *J. Phys. Chem. Lett.*, 2010, **1**, 3506–3509.
10 N. Uekawa, T. Kudo, F. Mori, Y. J. Wu and K. Kakegawa, *J. Colloid Interface Sci.*, 2003, **264**, 378–384.
11 A. I. Carrillo, J. García-Martínez, R. Llusar, E. Serrano, I. Sorribes, C. Vicent and J. Alejandro Vidal-Moya, *Microporous Mesoporous Mater.*, 2012, **151**, 380–389.
12 Y. Rao, M. Trudeau and D. Antonelli, *J. Am. Chem. Soc.*, 2006, **128**, 13996–13997.
13 M. Yurdakoc, M. Akcay, Y. Tonbul and K. Yurdakoc, *Turk. J. Chem.*, 1999, **23**, 319–327; I. Matsuzaki, M. Nitta and K. Tanabe, *J. Res. Inst. Catal., Hokkaido Univ.*, 1969, **17**, 46–53.
14 V. Meynen, P. Cool and E. F. Vansant, *Microporous Mesoporous Mater.*, 2009, **125**, 170–223.
15 M. Yurdakoc, M. Akcay, Y. Tonbul and K. Yurdakoc, *Turk. J. Chem.*, 1999, **23**, 319–327.
16 M. Tomasulo, S. Sortino, A. J. P. White and F. M. Raymo, *J. Org. Chem.*, 2005, **70**, 8180–8189; M. Tomasulo, S. Sortino and F. M. Raymo, *Org. Lett.*, 2005, **7**, 1109–1112.
17 M. Petriella, E. Deniz, S. Swaminathan, M. J. Roberti, F. M. Raymo and M. L. Bossi, *Photochem. Photobiol.*, 2013, **89**, 1391–1398; S. Swaminathan, M. Petriella, E. Deniz, J. Cusido, J. D. Baker, M. L. Bossi and F. M. Raymo, *J. Phys. Chem. A*, 2012, **116**, 9928–9923; E. Deniz, M. Tomasulo, J. Cusido, I. Yildiz, M. Petriella, M. L. Bossi, S. Salvatore and F. M. Raymo, *J. Phys. Chem. C*, 2012, **116**, 6058–6068.
18 S. Corrent, P. Hahn, G. Pohlers, T. J. Connolly, J. C. Scaiano, V. Fornés and H. García, *J. Phys. Chem. B*, 1998, **102**, 5852–5858.
19 G. L. Hallett-Tapley, C. O. L. Crites, M. Gonzalez-Bejar, K. L. McGilvray, J. C. Netto-Ferreira and J. C. Scaiano, *J. Photochem. Photobiol., A*, 2011, **224**, 8–15; D. A. Skoog, F. J. Holler and T. A. Nieman, *Principles of Instrumental Analysis*, Harcourt Brace & Company, Orlando, FL, 5th edn, 1998.
20 B. Fu, F. E. Curry and S. Weinbaum, *Am. J. Physiol.*, 1995, **269**, H2124–H2140.

